Pressure Output Feedback Control of Tollmien–Schlichting Waves in Falkner–Skan Boundary Layers

Tol, Henry; Kotsonis, Marios; de Visser, Coen

DOI
10.2514/1.J057010

Publication date
2019

Document Version
Accepted author manuscript

Published in
AIAA Journal: devoted to aerospace research and development

Citation (APA)
Tol, H., Kotsonis, M., & de Visser, C. (2019). Pressure Output Feedback Control of Tollmien–Schlichting Waves in Falkner–Skan Boundary Layers. *AIAA Journal: devoted to aerospace research and development*, *57*(4), 1538-1551. https://doi.org/10.2514/1.J057010

Pressure Output Feedback Control of Tollmien–Schlichting Waves in Falkner–Skan Boundary Layers

H.J. Tol* and M. Kotsonis† and C.C. de Visser‡
Delft University of Technology, 2629 HS Delft, The Netherlands

This paper investigates the use of point wall pressure measurements for output feedback control of Tollmien-Schlichting waves in Falkner-Skan boundary layers. A new approach is presented for input-output modeling of the linear dynamics of the fluid system and the integration with $\mathcal{H}_2$/LQG reduced-order control design. The pressure output at the wall is related with the global perturbation velocity field through the linearized pressure Poisson equation. A Kalman filter is subsequently used to obtain time-resolved estimates of the velocity field using pressure information at discrete points at the wall. The estimated field is in turn used to calculate an optimal state feedback control to suppress the instabilities. The controller is designed in both a feedforward, a feedback and a combined feedforward/feedback actuator/sensor configuration. It is shown that combined feedforward/feedback control gives the best trade-off between robust performance and robust stability in the presence of uncertainties in the Reynolds number and the pressure gradient. Robust performance in off-design conditions is enhanced compared to feedforward control while robust stability is enhanced compared to feedback control.

Nomenclature

$\mathcal{A}$, $\mathcal{B}$, $\mathcal{C}$, $\mathcal{D}$	=	full order /spatial continuous state-space operators
A, **B**, **C**, **D**	=	reduced order state-space matrices
E	=	perturbation energy
F	=	state feedback gain
f	=	body force vector
$\mathcal{L}$	=	linearized Navier-Stokes operator
L	=	Kalman filter gain
l	=	control penalty
m	=	dimensionless constant characterizing the pressure gradient

*Researcher, Faculty of Aerospace Engineering, h.j.tol@tudelft.nl
†Assistant Professor, Faculty of Aerospace Engineering, m.kotsonis@tudelft.nl
‡Assistant Professor, Faculty of Aerospace Engineering, c.c.devisser@tudelft.nl

p	=	fluctuating pressure
p_{ff}	=	feedforward pressure measurement
p_{fb}	=	feedback pressure measurement
Re_δ	=	Reynolds number based on local δ^*
Re_0	=	Reynolds number based on inflow δ^*
r	=	order of the reduced order model
$\mathbf{T}$	=	closed-loop transfer function
t	=	time
U_∞	=	dimensionless external free-stream velocity
$\boldsymbol{u}$	=	fluctuating velocity vector
$\boldsymbol{U}$	=	base flow vector
w	=	external disturbance
$\boldsymbol{x}$	=	dimensionless spatial coordinate
z, q, p_m	=	output signals
$\mathcal{Z}$	=	boundary to domain lifting operator
δ^*	=	displacement thickness, m
ξ	=	similarity variable
ϕ	=	control input
ν	=	kinematic viscosity, m^2/s
η	=	temporal state defined at the boundary
γ	=	estimation penalty, relative magnitude of the sensor noise
ω	=	radial frequency
ω_n	=	natural frequency
ζ	=	damping ratio
Γ	=	boundary
Subscripts		
in, out, wall	=	inflow boundary, outflow boundary, rigid wall
h, c, d,	=	homogeneous, control, disturbance
m, ff, fb,	=	measured, feedforward, feedback
Superscripts		
e	=	extended
$*$	=	dimensional variable

I. Introduction

Advances in actuator and sensor technologies that can sense/manipulate fluid flows on very short time and length scales have motivated the field of closed-loop flow control. In closed-loop control real-time sensor information is used to devise controls that alter the flow towards a desired state. In practice, measurements are non-ideal (noisy) and available only in a small portion of the system. Dynamic estimation strategies filter the available information using the governing equations, to extract the signal and to reconstruct the state of the system. The estimated state can subsequently be used within a state feedback control law. The combination of model-based estimation and control has gained significant attention for flow control [1–3] and is commonly referred to as an output feedback controller or a dynamic compensator [4–8]. In this study, pressure-based compensators are designed to suppress two-dimensional Tollmien-Schlichting (TS) wavepackets in laminar Falkner-Skan flows. The compensator approach in this study can be classified as a white box/gray box approach in which the model is a-priori based on the physics of the system, in this case the linearized Navier-Stokes equations (LNSE). Such model-based techniques provide important insights into the instability mechanisms that have to be addressed and potentially lead to the best possible performance with stability guarantees. For a recent and extensive review on control of transition and turbulence, also including so-called black-box and model-free approaches, the reader is referred to Brunton and Noack [9]. Three crucial aspects to achieve practical implementation of compensators are the computational cost for real-time application, robustness to model uncertainties and the integration of physically realizable actuators/sensors that are localized in space, which are discussed next.

A. Model reduction and control of convective instabilities

To address the computational aspects and to account for localised actuators and sensors, reduced-order models (ROM) have been extensively used in the design of compensators. Many techniques are available for model reduction of fluid flows which commonly involve the projection of the high-order system on a lower dimensional subspace. We refer to [10] for a recent review on model reduction methods for flow analysis and control. It is accepted that for control design purposes, projection on controllable and observable subspaces, formed by so-called balanced modes, produces the most reliable models with superior performance [10–13]. Balanced truncation [14] is widely used in control theory to extract the most controllable and observable modes of the system. However, exact balanced truncation is computationally intractable for high-order systems, e.g. if $n > 10^5$. For flow control purposes snapshot-based (white box) balanced truncation [15] and input-output-based (black-box) truncation using the eigensystem realization algorithm (ERA) [16, 17] are widely used. Both aim to construct approximate balanced reduced order models that capture the input-output behavior of the system, similar to exact balanced truncation.

To account for spatially localized actuators/sensors in the control design, Bagheri et al. [7] were the first to rigorously combine balanced model reduction with $\mathcal{H}_2$/LQG closed-loop control for convective instabilities in 2-D bound-

ary layer flows. The control design considered the use of in-domain volume forcing actuation and in-domain velocity measurements. This approach was extended in Bagheri et al. [18] to include wall shear measurement and wall actuation by means of localized suction and blowing. A generalization of the work of Bagheri et al. [7] to 3-D flows is presented in Semeraro et al. [19] and was applied by Semeraro et al. [20] in fully non-linear simulations to verify the possibility of delaying transition to turbulence using velocity measurements and volume forcing actuation. Limitations related to a more realistic set-up were addressed by Dadfar et al. [8, 21] for 2-D boundary layer flows. They integrated experimentally identified models of plasma actuators and physical actuator constraints were taken into account in the control design. Using plasma actuators and hot-wire velocity measurements Fabbiane et al. [22] demonstrated, for the first time, suppression of disturbances in wind-tunnel experiments using 2-D model-based LQG compensators, without any model fitting or system identification.

Fabbiane et al. [22] also stressed the robust performance issues of 2-D model-based LQG controllers in a feedforward actuator/sensor configuration in which the sensors are placed upstream of the actuators. Such a setup is commonly recommended for $\mathcal{H}_2$/LQG optimal control of convective instabilities as reviewed by Sipp and Schmid [3], Schmid and Sipp [23]. It guarantees robust stability in convective flows and the best nominal performance [3, 23, 24]. However, the performance of feedforward control deteriorates quickly in off-design conditions as shown in Fabbiane et al. [22] and feedforward control poses challenges in the presence of additional unmodeled dynamics and disturbances as argued by Belson et al. [24]. Therefore, a feedback configuration in which the sensor senses the effect of the actuator may be desirable in order to account for uncertainties. For example, Fabbiane et al. [22] experimentally applied adaptive filtered-x-least-mean-squares control to improve the performance in off-design conditions for the freestream velocity and Belson et al. [24] applied proportional-integral feedback control to recover the performance in the presence of unmodeled disturbances.

B. Pressure-based estimation

Currently localized (white/gray) model-based compensators for transition delay have either used velocity measurements or shear measurements for estimation of the perturbation field. Although, hot wire anemometry and hot film sensors can be effective for closed-loop control [22, 25], they can become problematic in practice. Hot wires are intrusive and the wires can break easily. Wall shear stress sensors are placed on the wall, but generally have a low signal to noise ratio, are not robust (temperature dependent, high mechanical stresses) and uncertainties are hard to quantify [26]. Pressure measurements on the other hand generally have a high signal-to-noise ratio and can be extracted remotely from the surface, e.g. using microphones embedded within a small cavity. The cavity does result in a loss of amplitude and phase and gives rise to Helmholtz resonances, which has to be accounted for.

Pressure measurements are commonly considered for control of global instabilities in free shear layer flows involving flow-induced noise/vibrations and flow-structure interaction. We refer to Cattafesta et al. [27] for an extensive

review on control of flow-induced cavity oscillations. Different variants (linear, quadratic, higher order) of static estimators, also known as stochastic estimation (SE) as originally introduced by Adrian [28], have been successfully applied for control in cavity flows [29, 30] and axisymmetric jets [31]. We refer to Lasagna et al. [32] for a recent overview of the SE technique, both for investigating the flow physics and the control applications. With SE the state estimate is represented by a static function of the sensors and the state estimate depends only on the measurements at the present time. This technique does not require a model, but requires a larger number of sensors, and is more sensitive to noise than dynamic model-based observers, such as the Kalman filter [15, 27, 31, 33]. Owing to the need for a ROM of the flow dynamics, preferably balanced, that relate the point pressure measurements with the model variables, dynamic state estimation is challenging. Models used for dynamic estimation/control which are based solely on the physics of the system have been obtained through POD/Galerkin projection in Sinha et al. [31], Rowley and Juttijudata [34], and balanced models from input-output data (black-box) using ERA have been obtained in Illingworth et al. [35, 36] for feedback control of flow resonances.

C. Objective and outline of the present study

Pressure sensors provide significant advantages over velocity or shear stress sensors in experimental applications. However, no attempt has yet been made to integrate point pressure measurements in the framework of (white/gray) model-based output feedback control for convective instabilities in boundary layer flows, which is the objective of the present study. To the best of our knowledge this is the first time that a localized pressure-based compensator is derived directly from the governing equations which is used to control instabilities in boundary layer flows. In addition, the control system is designed in both a feedforward, a feedback and a combined feedforward/feedback actuator/sensor configuration. The performance of the three configurations is compared in both nominal and off-design conditions. A feedback configuration was first considered in Belson et al. [24] who showed robustness to unmodeled external disturbances using PI control. In the present study the robustness is evaluated in the presence of parametric uncertainties in the Reynolds number and the pressure gradient.

The use of pressure measurements for dynamic flow estimation is not trivial. Firstly, for modeling of wall-bounded shear flows, the pressure is commonly eliminated from the state equations (also in this study) by formulating the linearized Navier-Stokes equations in a divergence free state-space, see e.g. Bagheri et al. [7, 18], Semeraro et al. [19], Jones et al. [37] and we refer to Bewley et al. [38] for a general framework. Due to the fact that pressure is eliminated from the model, estimation for correlating the model variables to the pressure measurements becomes less trivial. Secondly the fluctuating pressure at a given point on the wall is related to the global velocity field (e.g. through the pressure-Poisson equation). As a result unmodeled disturbances as well as dynamic uncertainties inherent in any ROM, can result in high uncertainties in the modeled pressure output. This puts more stringent constraints on accurately modeling of the input-output behavior.

To address these challenges a new two-step approach is proposed for the input-output modeling of the *linear* dynamics, which is integrated with $\mathcal{H}_2$/LQG reduced-order controller design. The dynamic state equation, which is required to design the state-feedback control law, is derived through a divergence-free projection of the linearized Navier-Stokes equations. The pressure output equation, which is required to dynamically estimate the velocity field, is subsequently derived through the linearized pressure-Poisson equation in a separate step, independently of the derivation of the state-equations. The controller is synthesized by making use of the framework recently presented in Tol et al. [39], which combines direct state-space discretization of governing equations using multivariate splines [40] with exact balanced truncation [14] to design low-order controllers. Tol et al. [39] also proposed a new physically motivated inflow disturbance model which allows for robust estimation of the perturbations within the localized domain that encapsulates the actuators and sensors. In Tol et al. [39] flow perturbations in a channel flow are estimated/controlled using wall shear measurements and localized suction and blowing at the wall in a feedforward configuration. They showed robustness to both unmodeled disturbances and truncated dynamics resulting from the model reduction step. In this work the framework from Tol et al. [39] is applied to Falkner-Skan flows and is extended by introducing point wall pressure measurements for the flow estimation in a feedforward/feedback configuration.

The outline of this paper is as follows. In Sec. B the governing equations are presented. In Sec. III the equations are written in state-space form and the finite-dimensional approximation is discussed. Section IV presents the inflow disturbance model, which is linked to the relevant flow physics, and is of importance for the estimation problem. The pressure is eliminated from the state equations by formulating the state equations in a divergence free basis. In Sec. V a new pressure output equation is derived which relates the upstream disturbances and the velocity perturbation field with the pressure at the measurement location at the wall. In Sec. VI the reduced order controller/estimator is designed within an $\mathcal{H}_2$/LQG optimal control framework. The controllers are evaluated in Sec. VII followed by conclusions in Sec. VIII.

II. Flow configuration

A. Overview set-up

2-D perturbations in an incompressible boundary layer flow over a flat plate are considered. The flow configuration, including the inputs-outputs, used in this study is shown in Fig. 1. Boundary layers behave as noise amplifiers of unknown upstream disturbances which trigger convective perturbations in a frequency broadband that amplify in both space and time as they propagate downstream. Tol et al. [39] presented a new inflow perturbation modeling which allows for efficient estimation and control of the perturbations within the localized control domain that encapsulates the actuators and sensors. The controller is synthesized using a localized computational domain which naturally avoids very large systems and allows a direct application of linear system theoretic tools for model reduction and control

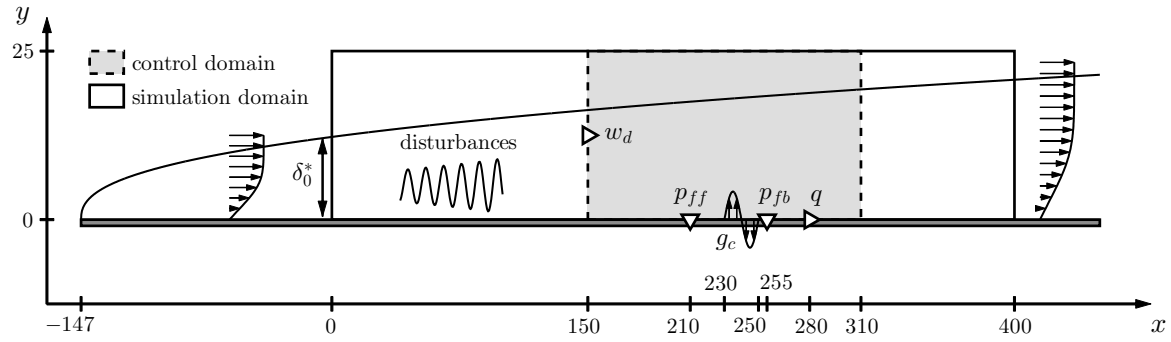

Fig. 1 Simulation domain, control domain and input-output configuration. Reference displacement thickness δ_0^*, inflow disturbance w_d, feedforward sensor p_{ff}, feedback sensor p_{fb}, controlled output q and actuator distribution g_c.

design. A larger simulation domain is used in order to properly evaluate the controller in Sec. VII.

For the control design external disturbance sources, modeled through $w_d(t)$, are assumed to enter the control domain through the inflow. The chosen control objective is to suppress the effect of inflow disturbances $w_d(t)$ on the wall shear stress fluctuations defined by the controlled output $q(t)$. The control actuation is achieved by localized wall-normal suction and blowing at the wall characterized by the distribution $g_c(x)$ and pressure sensors are used to extract the measurement information at the wall. Three actuator/sensor configurations are considered, which are a feedforward configuration, a feedback configuration and a combined feedforward/feedback configuration. In the feedforward actuator/sensor configuration the sensor is placed upstream of the actuator to detect the upcoming perturbations. Due to the convective nature of the flow, this setup dynamically corresponds to disturbance feedforward control. In the feedback configuration the sensor is placed downstream of the actuator such that the effect of the actuator is fed back to the controller. The feedback sensor is placed close to the actuator ($x_{fb} = 255$) in order to have sufficient observability of the TS waves in the actuator domain and to limit the effect of time delays [24]. All three configurations are a special case of output feedback control within the optimal control framework formalized by Doyle et al. [41]. In Sec. B the flow domain and the governing equations are presented. The inputs and outputs will be discussed in the next sections.

B. Governing equations

The dynamics of the perturbations are obtained by linearizing the Navier-Stokes equations around the steady boundary layer. The boundary layer is approximated by a profile from the family of Falkner-Skan similarity solutions. It is assumed that the outer free-stream velocity is given by $U_\infty^* = U_0^*(x^*/x_0^*)^m$ with x_0^* a fixed physical position from the virtual leading edge of the plate and U_0^* the free-stream velocity at that position. The asterisk (*) is used to denote a dimensional variable. The parameter m characterizes the pressure gradient, both favorable ($m > 0$) and adverse pressure gradients ($m < 0$) can be accounted for. The boundary layer displacement thickness δ_0^* and the free-

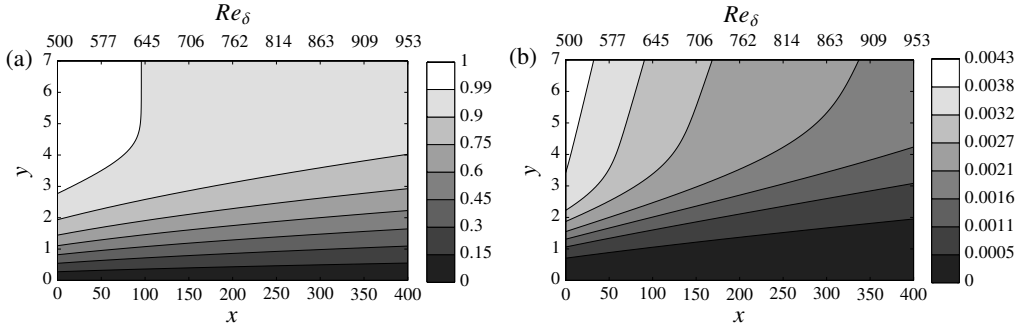

Fig. 2 Falkner-Skan boundary layer ($m = -0.02$, $Re_0 = 500$) used for the linearization. (a) streamwise component U. (b) wall-normal component V.

stream velocity U_0^* at $x^* = x_0^*$ are chosen as reference variables to non-dimensionalize the flow with corresponding Reynolds number $Re = Re_0 = \frac{U_0^* \delta_0^*}{\nu}$ where ν is the kinematic viscosity. For the nominal simulation case and control design case we select $Re = 500$, $m = -0.02$ which corresponds to a distance of $x_0^* = 147\delta_0^*$ from the virtual leading edge. The computational domain is also scaled with δ_0^* and the non-dimensional coordinates are defined as $x = (x^* - x_0^*)/\delta_0^*$, $y = y^*/\delta_0^*$. For flow simulations the domain $x_{sim} \in [0, 400]$, $y_{sim} \in [0, 25]$ is considered. The controller is synthesized using localized computations within the domain $x_c \in [150, 310]$, $y_c \in [0, 25]$. Based on the following similarity variable $\xi(\boldsymbol{x}^*) = y^* \sqrt{U_\infty^*/\nu x^*}$, the boundary layer in these domains is obtained by solving the Falkner-Skan equation

$$f''' + \frac{m+1}{2} f f'' + m(1 - f'^2) = 0, \quad f(0) = f'(0) = 0,\ f'(\infty) = 1. \tag{1}$$

The solutions for $f(\xi)$ and $f'(\xi)$ are combined into the non-dimensional velocity profiles

$$U(\boldsymbol{x}) = \frac{U^*}{U_0^*} = U_\infty f'(\xi), \tag{2}$$

$$V(\boldsymbol{x}) = \frac{V^*}{U_0^*} = \frac{1}{2\varrho} \sqrt{\frac{U_\infty}{(x + x_0) x_0}} \Big((1 - m)\xi f'(\xi) - (1 + m) f(\xi) \Big), \tag{3}$$

with $\xi(\boldsymbol{x}) = \varrho \sqrt{U_\infty \frac{x_0}{x + x_0}}\, y$, $\varrho = \int_0^\infty (1 - f') \mathrm{d}\xi$ and $U_\infty = U_\infty^*/U_0^* = (x/x_0 + 1)^m$. The displacement thickness for this boundary layer is given by $\delta^* = \int_0^\infty (1 - U^*/U_\infty^*)\, \mathrm{d}y^* = \sqrt{\nu x^*/U_\infty^*}\, \varrho$, and the local Reynolds number Re_δ at a particular x station can subsequently be computed using

$$Re_\delta = Re \sqrt{\left(1 + \frac{\varrho^2 x}{Re}\right) U_\infty}. \tag{4}$$

Figure 2 shows the boundary layer in Eqs. (2) and (3) along with the local Reynolds numbers [Eq. (4)]. Small

perturbations to the boundary layer are governed by the linearized Navier-Stokes equations (LNSE). Let $\boldsymbol{U}(\boldsymbol{x})+\boldsymbol{u}(\boldsymbol{x},t)$ be the perturbed velocity field. The linearized non-dimensional equations, including the boundary conditions used in this study, are given by

$$\frac{\partial \boldsymbol{u}}{\partial t} = \underbrace{-(\boldsymbol{U}\cdot\boldsymbol{\nabla})\,\boldsymbol{u} - (\boldsymbol{u}\cdot\boldsymbol{\nabla})\,\boldsymbol{U} + \frac{1}{Re}\Delta\boldsymbol{u}}_{\mathcal{L}\boldsymbol{u}} - \boldsymbol{\nabla}p + \boldsymbol{f}, \tag{5a}$$

$$0 = \boldsymbol{\nabla}\cdot\boldsymbol{u}, \tag{5b}$$

$$\boldsymbol{u}|_{\Gamma_{wall}} = \boldsymbol{u}_c, \tag{5c}$$

$$\boldsymbol{u}|_{\Gamma_{in}} = \boldsymbol{u}_d, \tag{5d}$$

$$\boldsymbol{u}|_{\Gamma_{fs}} = 0, \tag{5e}$$

$$0 = -\boldsymbol{n}p|_{\Gamma_{out}} + \frac{1}{Re}(\boldsymbol{n}\cdot\boldsymbol{\nabla})\,\boldsymbol{u}|_{\Gamma_{out}}, \tag{5f}$$

where $\mathcal{L}$ is the linearized Navier-Stokes operator, $\boldsymbol{u}(\boldsymbol{x},t) = [u(\boldsymbol{x},t),\ v(\boldsymbol{x},t)]$ and $p(\boldsymbol{x},t)$ denote the velocity and pressure perturbation field and $\boldsymbol{f}(\boldsymbol{x},t)$ is body force field per unit mass. In-domain body forces are typically used for applying control. In this study only wall-actuation is considered, which is modeled through the boundary condition. Without loss of generality the body force will be set to zero in the remainder of the paper. The system is closed by the boundary conditions in Eqs. (5c)-(5f). Dirichtlet boundary conditions are prescribed on $\Gamma_D = \Gamma_{wall} \cup \Gamma_{in} \cup \Gamma_{fs}$ where Γ_{wall} is the rigid wall boundary, Γ_{in} is the inflow boundary and Γ_{fs} is the external freestream boundary. $\boldsymbol{u}_c$ is the prescribed velocity input profile at the wall Γ_{wall} which is used to model the wall-actuation (see next section). $\boldsymbol{u}_d$ is the inflow disturbance velocity used to account for unknown external disturbances in the control design. The inflow boundary condition is only imposed in the control model and is discussed in detail in Sec. IV as it is an integral part of the control design. An unperturbed flow is assumed at the computational inflow of the simulation domain ($\boldsymbol{u}(0,y) = 0$)). For both cases it is assumed that the perturbations vanish at the upper freestream boundary Γ_{fs} ($\boldsymbol{u}(x,25) = 0$). At the outflow boundary Γ_{out} a standard Robin boundary condition [Eq. (5d)] is prescribed, which has proven to be well suited for uni-directional outflows [42]. The outflow condition is implicitly satisfied by the variational formulation used to discretize the LNSE and does not need to be explicitly taken into account.

III. State-space formulation

In order to apply linear control theoretic tools the flow equations must be formulated into the standard state-space form. To generalize the modeling approach and control system design the equations are written as an abstract equation in operator form [38, 43]. Explicit discrete expressions are obtained for all operators which are discussed afterwards.

A. State equations

The pressure term, along with the divergence equation can be eliminated by the projection of the equations onto the divergence free space [38]. This avoids dealing with a singular descriptor state-state system and allows straightforward application of classical control theoretic tools [37]. Actuation [Eq. (5c)] and disturbance [Eq. (5d)] are both introduced through the boundary which renders the system in-homogeneous. Both actuation and disturbance are mathematically equivalent. By a standard lifting procedure [38, 44] the effect of the boundary condition can be represented by a volume forcing in a modified state-space system with homogeneous boundary conditions. We also refer to [43, Section 3.3] for more information about this formulation. The in-homogeneous boundary conditions can be lifted by setting

$$\boldsymbol{u} = \boldsymbol{u}_h + \mathcal{Z}_c \boldsymbol{u}_c + \mathcal{Z}_d \boldsymbol{u}_d, \tag{6}$$

where $\boldsymbol{u}_h$ is a solution of the homogeneous problem and $\mathcal{Z}_c, \mathcal{Z}_d$ 'lift' the boundary conditions to the interior of the domain and must be defined such that $(\mathcal{Z}_c \boldsymbol{u}_c)\,|_{\Gamma_D} = \boldsymbol{u}_c$ and $\nabla \cdot (\mathcal{Z}\boldsymbol{u}_c) = 0$ [38, 43]. Let $\mathcal{X} = \{\boldsymbol{u} \in L^2(\Omega)^2 |\ \nabla \cdot \boldsymbol{u} = 0\}$ and let $\mathcal{P}$ be an orthogonal projector from $L^2(\Omega)^2 \mapsto \mathcal{X}$ satisfying $\mathcal{P}\boldsymbol{u} = \boldsymbol{u}$ and $\mathcal{P}(\nabla p) = 0$. Applying the projection $\mathcal{P}$ to Eq. (5a) and substituting the change of variables [Eq. (6)] gives the following homogeneous equation in operator form

$$\dot{\boldsymbol{u}}_h = \mathcal{A}\boldsymbol{u}_h + \mathscr{A}\mathcal{Z}_c \boldsymbol{u}_c - \mathcal{Z}_c \dot{\boldsymbol{u}}_c + \mathscr{A}\mathcal{Z}_d \boldsymbol{u}_d - \mathcal{Z}_d \dot{\boldsymbol{u}}_d, \tag{7}$$

where $\mathscr{A}\boldsymbol{u} = \mathcal{P}\mathcal{L}\boldsymbol{u}$, $\mathcal{A}\boldsymbol{u} = \mathscr{A}\boldsymbol{u}$ for $\boldsymbol{u} \in \mathcal{D}(\mathcal{A})$ and the domain $\mathcal{D}(\mathcal{A})$ includes homogeneous boundary conditions $\mathcal{D}(\mathcal{A}) = \{\boldsymbol{u} \in \mathcal{X} \mid \boldsymbol{u}|_{\Gamma_D} = 0\}$. The external input (disturbance and control) in Eq. (7) are actually the time derivative of the prescribed velocity at the boundary. Actuation and disturbance are independent of each other and the spatio-temporal boundary actuator/disturbance model can be described by

$$\begin{aligned}
\begin{bmatrix} \dot{\boldsymbol{\eta}}_c \\ \dot{\boldsymbol{\eta}}_d \end{bmatrix} &= \begin{bmatrix} \mathcal{A}_c & 0 \\ 0 & \mathcal{A}_d \end{bmatrix} \begin{bmatrix} \boldsymbol{\eta}_c \\ \boldsymbol{\eta}_d \end{bmatrix} + \begin{bmatrix} \mathcal{B}_c \\ 0 \end{bmatrix} \phi + \begin{bmatrix} 0 \\ \mathcal{B}_d \end{bmatrix} w_d, \\
\begin{bmatrix} \boldsymbol{u}_c \\ \boldsymbol{u}_d \end{bmatrix} &= \begin{bmatrix} C_c & 0 \\ 0 & C_d \end{bmatrix} \begin{bmatrix} \boldsymbol{\eta}_c \\ \boldsymbol{\eta}_d \end{bmatrix},
\end{aligned} \tag{8}$$

with $\boldsymbol{\eta}_c(t)$, $\boldsymbol{\eta}_d(t)$ respectively the temporal state at the wall and inflow boundary, $\phi(t)$ the control input, $w_d(t)$ the external disturbance input and $\boldsymbol{u}_c(\boldsymbol{x},t)$, $\boldsymbol{u}_d(\boldsymbol{x},t)$ respectively the output velocity at the wall and inflow boundary. The inflow disturbance model $(\mathcal{A}_d, \mathcal{B}_d, C_d)$ is discussed in detail in the next section. To manipulate the flow, localized unsteady blowing and suction is considered that influences the wall-normal component at the wall. It is assumed that

the actuator dynamics are described by

$$\begin{aligned}\dot{\boldsymbol{\eta}}_c &= \tau^{-1}\left(\phi - \boldsymbol{\eta}_c\right) = \mathcal{A}_c\boldsymbol{\eta}_c + \mathcal{B}_c\phi,\\ \boldsymbol{u}_c &= \boldsymbol{g}_c\boldsymbol{\eta}_c = C_c\boldsymbol{\eta}_c,\end{aligned} \tag{9}$$

with $\boldsymbol{\eta}_c(t)$ the temporal actuator state that describes the amplitude of the blowing and suction. The temporal dynamics are governed by a simple first order lag filter with τ the time constant. The time constant is set equal to the sampling time of the simulations. In this case the filter corresponds to a stable approximation of a pure integrator commonly used for boundary control [6, 45]. A localized spatial distribution is considered with $\boldsymbol{g}_c(x) = [0,\ g_{c_v}]^T$ where $g_{c_v} = \sin\left(2\pi(x - x_g)/L_g\right)$ if $x_g \leq x \leq x_g + L_g$ and $g_{c_v} = 0$ elsewhere. The spatial length is set to $L_g = 20$ starting at $x_g = 230$. The spatial length is chosen to be less than the spatial wave-length of the dominant TS-waves (see next section) and allows for effective control over a broad frequency spectrum. Combining the boundary dynamics in Eq. (8) with the dynamics in the interior of the domain in Eq. (7) and using $\dot{\boldsymbol{u}}_c = C_c\mathcal{A}_c\boldsymbol{\eta}_c + C_c\mathcal{B}_c\phi$ it is straightforward to express Eq. (7) in the (extended) state-space form

$$\dot{\boldsymbol{u}}^e = \bar{\mathcal{A}}\boldsymbol{u}^e + \bar{\mathcal{B}}_c\phi + \bar{\mathcal{B}}_d w_d, \tag{10}$$

$$\boldsymbol{u}^e = \begin{bmatrix}\boldsymbol{u}_h\\ \boldsymbol{\eta}_c\\ \boldsymbol{\eta}_d\end{bmatrix}, \quad \bar{\mathcal{A}} = \begin{bmatrix}\mathcal{A} & \mathscr{A}\mathcal{Z}_cC_c - \mathcal{Z}_cC_c\mathcal{A}_c & \mathscr{A}\mathcal{Z}_dC_d - \mathcal{Z}_dC_d\mathcal{A}_d\\ 0 & \mathcal{A}_c & 0\\ 0 & 0 & \mathcal{A}_d\end{bmatrix}$$

$$\bar{\mathcal{B}}_c = \begin{bmatrix}-\mathcal{Z}_cC_c\mathcal{B}_c\\ \mathcal{B}_c\\ 0\end{bmatrix}, \quad \bar{\mathcal{B}}_d = \begin{bmatrix}-\mathcal{Z}_dC_d\mathcal{B}_d\\ 0\\ \mathcal{B}_d\end{bmatrix},$$

where $\boldsymbol{u}^e$ denotes an extended state. The output equation for the wall pressure measurements will be derived in Sec. V. This equation is less trivial since the pressure is eliminated from the state equations.

B. finite-dimensional approximation

Equation (10) represents the continuous formulation of the system. For simulation and control design a finite-dimensional approximation of Eq. (10) is required. The state-space modeling framework for parabolic PDEs from Tol et al. [40] is used, which was extended to fluid flows in [39]. The method uses projection with multivariate B-splines of arbitrary degree and smoothness defined on triangulations [46–48] to find matrix representations of all operators in Eq. (10). It has the geometrical flexibility of the finite element method and the approximation power of spectral

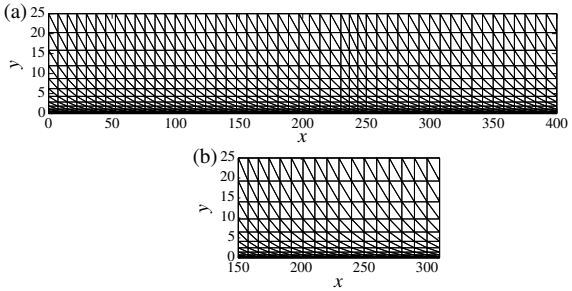

Fig. 3 Triangulations used for the (a) simulation model (1200 elements) and the (b) control model (340 elements).

methods. The pressure is eliminated from the equations by using a space of velocity fields which is divergence free and a suitable choice of variational formulation [39]. By expanding the solution in the null basis of the discrete divergence operator a minimal support basis is obtained for a divergence free spline space $\mathcal{S} \subset \mathcal{X}$. The system is projected on this basis through the variational formulation to obtain the finite-dimensional system. The triangulations used to construct the simulation model and the initial model that is used for model reduction and control design are shown in Fig. 3. To derive the simulation model a structured triangulation consisting of 1200 elements is used. It is refined near the wall using a hyperbolic stretching function to properly resolve the shear features. C^0 continuous elements and high degree, fifth order B-form polynomials are chosen which allow for better approximation properties [49]. The simulation model has a total of 11501 states. The model order already includes a large initial reduction resulting from the elimination of the divergence free constraint through the null basis expansion, which is equal to rank of the discrete divergence operator. It is verified with a mesh convergence analysis that higher resolutions did not provide an improved accuracy of the simulation results. To construct the initial model that is used for model reduction and control design a lower order discretization is used. Again C^0, $d = 5$ elements are chosen, but a coarser mesh consisting of 340 elements is used. The control model has 3231 states which allows efficient application of control theoretic tools for model reduction and control design. In the next sections the notation $(\mathcal{A}, \mathcal{B}, \mathcal{C}, \mathcal{D})$ is used to denote the full-order finite-dimensional system and the notation $(\mathbf{A}, \mathbf{B}, \mathbf{C}, \mathbf{D})$ is used to denote a reduced-order model.

IV. Inflow disturbance model

The state-space description [Eq. (10)] also includes a disturbance model, defined by $(\mathcal{A}_d, \mathcal{B}_d, \mathcal{C}_d)$, to account for external disturbances in the control design. The external disturbance sources are not precisely known in real environments and modeling assumptions have to made for the design of the controller. In particular the performance of state estimator relies on the model for the external disturbances as the estimation error is minimized in the presence of these disturbances. In addition, when model reduction is used in the design of the controller, the spatio-temporal structures that are retained in the model and that can be estimated in the control (actuators/sensors) domain depend on the

spatial-temporal structures that are excited by the external disturbances. For the control design external disturbances are introduced through the inflow boundary $\boldsymbol{u}|_{\Gamma_{in}} = \boldsymbol{u}_d$ with $\boldsymbol{u}_d$ the inflow perturbation velocity. In Tol et al. [39] a new inflow disturbance model is proposed which allows for efficient estimation of the dominant flow perturbations within the localized control region. This model is applied in this study for estimation of TS waves and is presented in this section. It should be noted that this model is independent of the disturbance scenario used to evaluate the controller in Sec. VII.

The inflow disturbance model is linked with the relevant flow physics through a classical local linear stability analysis [50] of the TS waves which will be discussed first. Linear stability theory assumes a locally parallel flow in which the individual perturbation modes (in the present case corresponding to TS waves) take the form

$$\boldsymbol{u} = \text{Real}\left[\tilde{\boldsymbol{u}} e^{\mathrm{i}(\alpha x - \omega t)}\right], \tag{11}$$

with $\tilde{\boldsymbol{u}}(y) = \tilde{\boldsymbol{u}}_r(y) + \mathrm{i}\tilde{\boldsymbol{u}}_i(y)$ the complex eigenfunction of the mode, $\alpha = \alpha_r + \mathrm{i}\alpha_i$ the complex wave-number and ω the real frequency of the mode. The modes are computed as solutions of the Orr-Sommerfeld (OS) equation using a local parallel spatial stability analysis at the inflow of the control domain, that is at $Re_0 = 500$ and $x = 150$ ($Re_\delta = 706$). Figure 4 shows the wavenumber (spatial eigenvalue) of the mode as function of the temporal frequency. Negative values for α_i characterize unstable modes. It can be observed that the modes are locally convectively unstable in a broad frequency band ($0.04 \leq \omega \leq 0.113$). To account for the dominant perturbation modes in a $\mathcal{H}_2$/LQG stochastic control framework, the following dynamic disturbance model is proposed by Tol et al. [39]

$$\begin{bmatrix} \dot{\eta}_d \\ \ddot{\eta}_d \end{bmatrix} = \underbrace{\begin{bmatrix} 0 & 1 \\ -\omega_n^2 & -2\zeta\omega_n \end{bmatrix}}_{\mathcal{A}_d} \underbrace{\begin{bmatrix} \eta_d \\ \dot{\eta}_d \end{bmatrix}}_{\boldsymbol{\eta}_d} + \underbrace{\begin{bmatrix} 0 \\ \omega_n^2 \end{bmatrix}}_{\mathcal{B}_d} w_d, \tag{12a}$$

$$\boldsymbol{u}_d = \underbrace{\begin{bmatrix} \tilde{\boldsymbol{u}}_r & -\frac{1}{\omega_{OS}}\tilde{\boldsymbol{u}}_i \end{bmatrix}}_{C_d} \begin{bmatrix} \eta_d \\ \dot{\eta}_d \end{bmatrix}, \tag{12b}$$

with $\boldsymbol{\eta}_d = [\eta_d, \dot{\eta}_d]$ the temporal state, $\boldsymbol{u}_d = \boldsymbol{u}|_{\Gamma_{in}}$ the perturbation velocity output at the inflow and w_d the external disturbance input assumed to be zero-mean Gaussian white noise with unit root-mean-square (rms) intensity

$$E\{w_d(t)\} = 0, \quad E\{w_d(t)w_d(\tau)\} = \delta(t-\tau). \tag{13}$$

The unity rms scaling will be discussed in more detail in Sec.VI. The disturbance model consist of a second-order low pass filter [Eq. (12a)] that accounts for the temporal dynamics of the Orr-Sommerfeld eigenfunction calculated at

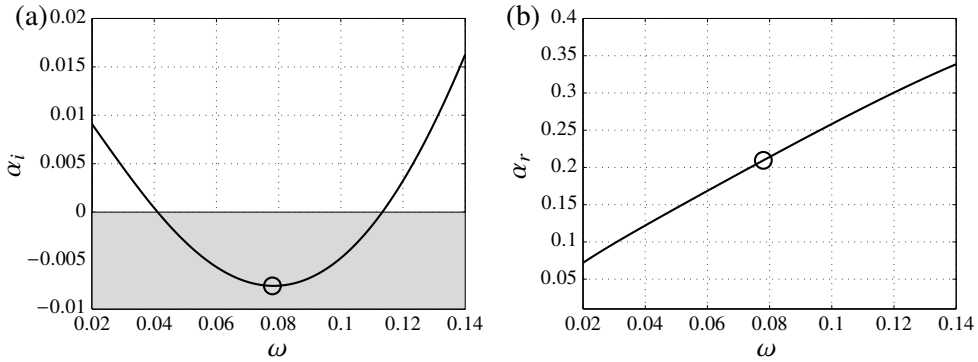

Fig. 4 The most unstable wavenumber as function of temporal frequency at $Re_0 = 500$, $x = 150$, $m = -0.02$. (a) The imaginary part. Negative values characterize unstable modes (gray region). (b) The real part.

the most amplified frequency ω_{OS}. For the nominal investigated conditions, the most amplified frequency is found at $\omega_{OS} = 0.078$, see Fig. 4. The shape of the eigenfuction at this frequency is shown in Fig. 5. The low-pass filter [Eq. (12a)] allows the magnitude frequency response shaping of $\boldsymbol{u}_d$ at the computational inflow to physically comply with the stability predictions. We choose $\zeta = 0.15$ and $\omega_n = 0.08$ such the filter has a peak frequency $\omega_p = \sqrt{1-2\zeta^2} = \omega_{OS}$ at the most amplified frequency and amplifies the magnitude of the disturbance w_d at this frequency with approximately a factor of 3.5. By increasing the magnitude of the temporal disturbance around this frequency, the controller will be better able to target the most unstable frequencies that contribute to transition, while at the same time achieving robustness at the higher and possibly unresolved frequencies. The temporal state is distributed at the inflow boundary through the output equation in Eq. (12b) where η_d excites the real part of the eigenfunction and $\dot{\eta}_d$ excites the imaginary part of the eigenfunction. The imaginary part is scaled with the mode frequency $\omega_{OS} = 0.078$ to account for the 90^o temporal phase difference of the imaginary and real part of the mode [39].

Although the spectrum of the Orr-Sommerfeld operator is continuous and unstable over a broad range of frequencies, only the most unstable perturbation mode is included in the model for control design. This model can easily be extended to include the excitation of Orr-Sommerfeld eigenfunctions calculated at different temporal frequencies. However, it is shown in Tol et al. [39] that a single mode disturbance model is effective for estimation of perturbations in a broad spatial and temporal bandwidth, which is also observed for the application case considered in this study. This can be attributed to the fact that the eigenfunction is excited over all frequencies in case of stochastic excitation. Also at other frequencies than the design frequency ω_{OS}, the inflow perturbation will quickly develop spatially to modal perturbations with different wavelengths and growth rates. The computational inflow is placed sufficiently far from the sensor location such that the non-modal and possible non-physical spatial transient behavior near the inflow does not contribute to the input-output behavior. The reader is referred to Tol et al. [39] for more information including a detailed spatio-temporal frequency response (input-output) analysis of the disturbance model.

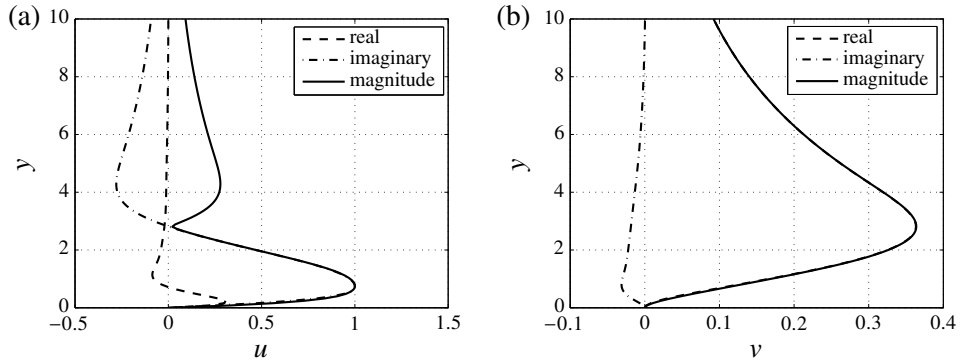

Fig. 5 The Orr-Sommerfeld eigenfunction for u (a) and v (b) calculated at $Re_0 = 500$, $x = 150$, $\omega = 0.078$, $m = -0.02$.

V. Pressure output equation

Information about the perturbations is extracted from wall pressure measurements. In this section the pressure output equation is derived which relates the model variables, i.e. the upstream disturbances and the velocity perturbation field, with the fluctuating pressure at the measurement location at the wall. The output equation is required to estimate the velocity field using a Kalman filter. The pressure output equation is derived from the linearized pressure Poisson equation (PPE). The PPE is commonly used to compute the pressure from the velocity field in the case when the pressure is eliminated from the field equations. For example, in pseudo spectral codes for incompressible flows such as SIMSON [51] that is commonly used for flow control. However, the application for dynamic flow estimation has so far not been reported. By using the PPE the pressure at the wall can be computed from the global velocity perturbation field. Taking the divergence of the linearized Navier-Stokes equations [Eq. (5a)] and exploiting Eq. (5b) yields the linearized PPE

$$\Delta p = \nabla \cdot \left(- \left(\boldsymbol{U} \cdot \boldsymbol{\nabla} \right) \boldsymbol{u} - \left(\boldsymbol{u} \cdot \boldsymbol{\nabla} \right) \boldsymbol{U} \right) . \tag{14}$$

At the boundary, the multiplication of Eq. (5a) with the wall outward normal $\boldsymbol{n}$ yields a Robin boundary condition for p. This condition and Eq. (14) defines the pressure uniquely up to an arbitrary constant. This constant does not affect the velocity field. To fix this constant it is assumed that the fluctuating pressure is zero at the top freestream boundary. This boundary condition replaces the Robin boundary condition on the freestream boundary. This results in the following boundary conditions for Eq. (14)

$$\frac{\partial p}{\partial \boldsymbol{n}} = \boldsymbol{n} \cdot \left(- \left(\boldsymbol{U} \cdot \boldsymbol{\nabla} \right) \boldsymbol{u} - \left(\boldsymbol{u} \cdot \boldsymbol{\nabla} \right) \boldsymbol{U} + \frac{1}{Re} \Delta \boldsymbol{u} - \dot{\boldsymbol{u}} \right) \qquad \text{on } \Gamma_{Robin} = \Gamma_{in} \cup \Gamma_{wall} \cup \Gamma_{out}, \tag{15}$$

$$p = 0 \qquad \text{on } \Gamma_{fs}. \tag{16}$$

To solve the pressure with the Robin and the Dirichlet boundary conditions the pressure is sought in

$$L_0^2(\Omega) = \left\{ p \in L^2(\Omega) | p = 0 \text{ on } \Gamma_{fs} \right\}. \tag{17}$$

The pressure can subsequently be computed as a solution of a minimization problem [49], namely minimizing

$$\begin{aligned} \mathcal{J}(p) = \frac{1}{2} \int_\Omega |\nabla p|^2 \, d\Omega + \int_\Omega \left(\nabla \cdot \left(- \left(\boldsymbol{U} \cdot \boldsymbol{\nabla} \right) \boldsymbol{u} - \left(\boldsymbol{u} \cdot \boldsymbol{\nabla} \right) \boldsymbol{U} \right) \right) p \, \mathrm{d}\Omega \\ - \int_{\Gamma_{Robin}} \left(- \left(\boldsymbol{U} \cdot \boldsymbol{\nabla} \right) \boldsymbol{u} - \left(\boldsymbol{u} \cdot \boldsymbol{\nabla} \right) \boldsymbol{U} + \frac{1}{Re} \Delta \boldsymbol{u} - \dot{\boldsymbol{u}} \right) \cdot \boldsymbol{n} p \, \mathrm{d}\Gamma \end{aligned} \tag{18}$$

over $L_0^2(\Omega)$. Equation (18) is discretized using a spline basis for $L_0^2(\Omega)$ defined on the same mesh as shown in Fig. 3. The pressure is subsequently computed by setting the gradient with respect to the pressure coefficients to zero. When the solution is evaluated on the measurement locations at the wall results in an output equation of the form

$$\boldsymbol{p}_m = C_u \boldsymbol{u} + C_{\dot{u}} \dot{\boldsymbol{u}} \tag{19}$$

since Eq. (18) is linear in both $\boldsymbol{u}$ and $\dot{\boldsymbol{u}}$. Applying the linear change of variables from Eq. (6) for $\boldsymbol{u}$ and substituting the state equations [Eq. (10)] for $\dot{\boldsymbol{u}}^e$ gives

$$\begin{aligned} \boldsymbol{p}_m &= \begin{bmatrix} C_u & C_u \mathcal{Z}_c C_c & C_u \mathcal{Z}_d C_d \end{bmatrix} \begin{bmatrix} \boldsymbol{u}_h \\ \boldsymbol{\eta}_c \\ \boldsymbol{\eta}_d \end{bmatrix} + \begin{bmatrix} C_{\dot{u}} & C_{\dot{u}} \mathcal{Z}_c C_c & C_{\dot{u}} \mathcal{Z}_d C_d \end{bmatrix} \begin{bmatrix} \dot{\boldsymbol{u}}_h \\ \dot{\boldsymbol{\eta}}_c \\ \dot{\boldsymbol{\eta}}_d \end{bmatrix} \\ &= \bar{C}_u \boldsymbol{u}^e + \bar{C}_{\dot{u}} \dot{\boldsymbol{u}}^e \\ &= \left(\bar{C}_u + \bar{C}_{\dot{u}} \bar{\mathcal{A}} \right) \boldsymbol{u}^e + \bar{C}_{\dot{u}} \bar{\mathcal{B}}_c \phi + \bar{C}_{\dot{u}} \bar{\mathcal{B}}_d w_d \\ &= \bar{C} \boldsymbol{u}^e + \bar{\mathcal{D}}_c \phi + \bar{\mathcal{D}}_d w_d. \end{aligned} \tag{20}$$

The external disturbance w_d and the control input ϕ affect the measured output instantly modeled by the feedthrough terms $\bar{\mathcal{D}}_d$ and $\bar{\mathcal{D}}_c$. Fig. 6 shows that value of the feedthrough terms evaluated at the wall. It can be observed that the instantaneous effect of the external input (control and disturbance) is localized and is diffused in the domain. The instantaneous effect of the inflow disturbance w_d on the measured outputs at $x = 210$ and $x = 255$ is negligible. For generality and possible extensions to other disturbance models, $\mathcal{D}_d$ is not omitted in the control design in the next section. The instantaneous effect of the control input on the measured outputs is not negligible, particularly for the feedback sensor. However, the dynamic effect of the control input on the feedforward sensor is small due to the convective nature of the flow, resulting in a transfer function characterized by a constant. To also account for sensor

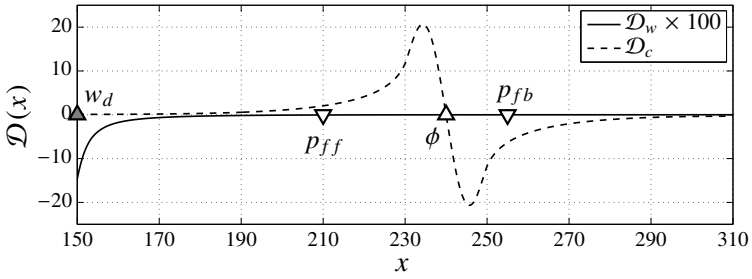

Fig. 6 $\mathcal{D}_w$ and $\mathcal{D}_c$ feed-through evaluated at the wall.

inaccuracies it is assumed that the measurement is corrupted by zero-mean Gaussian white noise w_n which modifies Eq. (20) to

$$\boldsymbol{p}_m = \bar{C}\boldsymbol{u}^e + \bar{\mathcal{D}}_c\phi + \bar{\mathcal{D}}_d w_d + \gamma w_n, \tag{21}$$

where γ_p reflects the magnitude of the uncertainty which can be tuned to design the controller.

VI. $\mathcal{H}_2$/LQG reduced order control design

The reduced-order controller is designed within an $\mathcal{H}_2$/LQG optimal control framework [41, 52] to account for the inflow disturbances and measurement noise. The controller is designed for the state-space system defined by the state equation (10) and the output equation (21). In addition a controlled output q is defined which is used as control objective to synthesize the controller. The complete input-output system can be formulated as

$$\begin{aligned} \dot{\boldsymbol{u}}^e &= \bar{\mathcal{A}}\boldsymbol{u}^e + \bar{\mathcal{B}}_c\phi + \bar{\mathcal{B}}_d w_d, \\ q &= \bar{C}_1\boldsymbol{u}^e, \\ \boldsymbol{p}_m &= \bar{C}_2\boldsymbol{u}^e + \bar{\mathcal{D}}_c\phi + \bar{\mathcal{D}}_d w_d + \gamma w_n, \end{aligned} \tag{22}$$

where $\boldsymbol{p}_m$ is the measured pressure from the feedforward sensor, the feedback sensor or both sensors, depending on the configuration. The controlled output is defined by

$$\begin{aligned} q = \bar{C}_1\boldsymbol{u} &= \int_{\Gamma_{wall}} h(x)\tau_{xy}|_{\Gamma_{wall}}\,\mathrm{d}x \\ &= \frac{1}{Re}\int_{\Gamma_{wall}} h(x)\partial_y u|_{\Gamma_{wall}}\,\mathrm{d}x, \end{aligned} \tag{23}$$

where $h(x)$ is chosen as a Gaussian distribution function $h(x) = \exp\left[-((x - x_q)/r_x)^2\right]$ with $x_q = 280$ the center of the distribution and $r_x = 5$ the radius. The wall shear stress fluctuations in Eq. (23) is found to be an effective and robust performance indicator for the input-output configuration considered in this study. The controlled output

is placed sufficiently far from the actuator (see also Fig. 1) such that the actuator has no direct influence on q and minimization of q is achieved by minimizing the effect of the inflow perturbations alone. However, it is found that there is not much sensitivity with respect to the choice of the position x_q and the radius r_x of the distribution, as long as it is placed sufficiently far from the actuator.

$\mathcal{H}_2$ optimal control theory considers the frequency domain interpretation of the cost function ($\mathcal{H}_2$ closed-loop system norm) while the LQG control theory considers the time-domain interpretation. Both theories are equivalent in the sense that the $\mathcal{H}_2$ control problem can be formulated as an equivalent LQG control problem and vice-versa [52]. In this section, the time-domain LQG cost function, is considered. The control objective is to suppress the wall shear stress fluctuations defined by q. The LQG cost function to design the controller is defined by

$$\begin{aligned} \mathcal{J}_{LQG} &= E\left\{\lim_{T\to\infty}\frac{1}{T}\int_0^T \boldsymbol{z}^T\boldsymbol{z}\,\mathrm{d}t\right\} \\ &= E\left\{\lim_{T\to\infty}\frac{1}{T}\int_0^T q^2 + l^2\phi^2\,\mathrm{d}t\right\}, \end{aligned} \tag{24}$$

with $\boldsymbol{z}(t) = [q(t),\, l\phi(t)]^T$ the performance measure to be minimized. Equation (24) also includes a penalty on the control input defined by the parameter l which determines the trade-off between a low controlled output power q^2 and a low control effort ϕ^2 in the design of the controller. The reduced-order controller that minimizes Eq. (24) is derived in two steps. First, a reduced-order model (ROM) is derived using balanced truncation [14]. Secondly, the ROM is used to synthesize the controller and the truncated dynamics are taken into account in the control system design. Balanced truncation extract the most controllable and observable modes of the system. It first involves a similarity transformation of the form $\boldsymbol{u}^e \mapsto \mathbf{S}\boldsymbol{u}^e$, which balances the system matrices through $\bar{\mathcal{A}} \mapsto \mathbf{S}\bar{\mathcal{A}}\mathbf{S}^{-1}$, $\bar{\mathcal{B}} \mapsto \mathbf{S}\bar{\mathcal{B}}$ and $\bar{\mathcal{C}} \mapsto \bar{\mathcal{C}}\mathbf{S}^{-1}$, $\bar{\mathcal{D}} \mapsto \bar{\mathcal{D}}$, such that each state has an equal measure for both controllability and observability. The reduced-order model of order r described by the matrices $\mathbf{A}$,$\mathbf{B}$,$\mathbf{C}$ and $\mathbf{D}$ is obtained from the balanced matrices by retaining the rows and columns corresponding to most controllable and observable states. Note that balanced truncation does not depend on $\bar{\mathcal{D}}$ and that $\bar{\mathcal{D}} = \mathbf{D}$. Also note that balanced truncation does not eliminate physical variables, it only makes a change of coordinates and represents the physical variables with a reduced-order representation. In other words the reduced-order balanced variables can be related back to the physical variables through the inverse of the similarity transformation $\boldsymbol{u}^e = \mathbf{S}_r^{-1}\boldsymbol{u}_r$, where $\mathbf{S}_r^{-1}$ are the first r columns of the inverse of the similarity transformation used to balance the system. This inverse transformation will be used to visualize the reduced-order state-estimates in Sec. VII.

The optimal controller based on the ROM combines a state estimator and a state feedback, and can be written as a dynamic system in the form

$$\begin{aligned} \dot{\hat{\boldsymbol{u}}}_r &= \mathbf{A}\hat{\boldsymbol{u}}_r + \mathbf{B}_c\,\phi + \mathbf{L}\left(\boldsymbol{p}_m - \mathbf{D}\phi - \mathbf{C}\hat{\boldsymbol{u}}_r\right), \\ \phi &= -\mathbf{F}\hat{\boldsymbol{u}}_r, \end{aligned} \tag{25}$$

with $\hat{\boldsymbol{u}}_r \in \mathbb{R}^r$ the estimated state and where $\mathbf{F}$, $\mathbf{L}$ are respectively the state feedback gain and the estimator (Kalman) gain to be optimized. Note that the observation $\tilde{\boldsymbol{p}}_m = \boldsymbol{p}_m - \mathbf{D}\phi$ is used for output feedback rather than $\boldsymbol{p}_m$ only, such that the controller can be synthesized based on $\tilde{\boldsymbol{p}}_m$, which fits into the standard form required to synthesize the controller [41]. Due to the well known separation property [52, pp. 388-390] of the optimal solution the state feedback and the state estimator can be designed and synthesized independently. The state feedback gain is obtained by minimizing Eq. (24) when noise is ignored. For the ROM this means to find $\mathbf{F}$ that minimizes

$$\mathcal{J} = \lim_{T\to\infty} \frac{1}{T} \int_0^T \boldsymbol{u}_r^T \mathbf{C}_1^T \mathbf{C}_1 \boldsymbol{u}_r + l^2\phi^2 \, \mathrm{d}t \tag{26}$$

subject to the closed-loop system dynamics $\dot{\boldsymbol{u}}_r = (\mathbf{A} - \mathbf{B}_c\mathbf{F})\,\boldsymbol{u}_r$. The Kalman gain $\mathbf{L}$ is subsequently obtained by minimizing the covariance of the estimated state

$$E\left\{(\boldsymbol{u}_r - \hat{\boldsymbol{u}}_r)^T(\boldsymbol{u}_r - \hat{\boldsymbol{u}}_r)\right\} = E\left\{\tilde{\boldsymbol{u}}_r^T\tilde{\boldsymbol{u}}_r\right\} \tag{27}$$

subject to the error dynamics $\dot{\tilde{\boldsymbol{u}}}_r = (\mathbf{A} - \mathbf{LC})\,\tilde{\boldsymbol{u}}_r + (\mathbf{B}_d - \mathbf{LD}_w)\,w_d - \mathbf{L}\gamma w_n$. Note that $\mathbf{L}$ is optimized to provide an optimal estimate in the presence of external disturbances w_d and w_n. For the control design the external disturbances are assumed to be Gaussian white noise with unit intensity. As a result the estimation problem is parameterized in terms of γ which reflects the uncertainty in the measurement. It can be shown that with this parameterization γ also reflects a rms value for the sensor noise relative to the state disturbances [53]. The optimal solutions for the control and estimation problem can be obtained independently by solving the associated algebraic Riccati equations for Eqs. (26) and (27) [52, ch.14, pp.375-377], which together form the compensator in Eq. (25). In the design of the compensator the parameters l and γ can independently be adjusted to achieve the desired closed-loop performance. However, no guarantees are available about the performance of the controller designed for the ROM on the original system. Therefore the truncated dynamics are taken into account by evaluating the performance of the controller in combination with the original system. Combining the compensator in Eq. (25) with the original system in Eq. (22) gives the following closed-loop system from the external disturbances to the performance measure $\boldsymbol{z}(t) = [q(t),\, l\phi(t)]^T$

$$\begin{aligned}
\begin{bmatrix} \dot{\boldsymbol{u}}^e \\ \dot{\hat{\boldsymbol{u}}}_r \end{bmatrix} &= \underbrace{\begin{bmatrix} \bar{\mathcal{A}} & -\bar{\mathcal{B}}_c\mathbf{F} \\ \mathbf{L}\bar{C} & \mathbf{A} - \mathbf{B}_c\mathbf{F} - \mathbf{LC} \end{bmatrix}}_{\mathcal{A}_{cl}} \begin{bmatrix} \boldsymbol{u}^e \\ \hat{\boldsymbol{u}}_r \end{bmatrix} + \underbrace{\begin{bmatrix} \bar{\mathcal{B}}_d & 0 \\ \mathbf{L}\bar{\mathcal{D}}_w & \mathbf{L}\gamma \end{bmatrix}}_{\mathcal{B}_{cl}} \begin{bmatrix} w_d \\ w_n \end{bmatrix}, \\
\boldsymbol{z} &= \underbrace{\begin{bmatrix} \bar{C}_1 & 0 \\ 0 & -l\mathbf{F} \end{bmatrix}}_{C_{cl}} \begin{bmatrix} \boldsymbol{u}^e \\ \hat{\boldsymbol{u}}_r \end{bmatrix}.
\end{aligned} \tag{28}$$

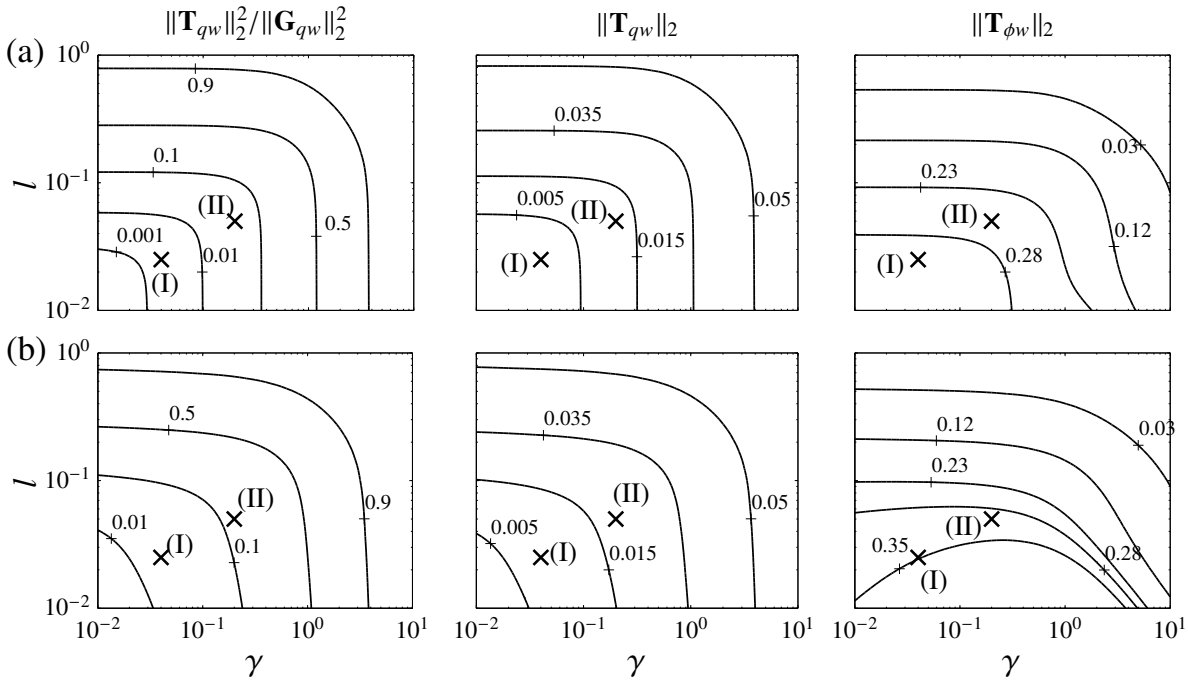

Fig. 7 Contours of the closed-loop system norms $\|\mathbf{T}_{qw}\|$ [Eq. (29)], $\|\mathbf{T}_{\phi w}\|_2$ [Eq. (30)] and the relative energy norm $\|\mathbf{T}_{qw}\|_2^2/\|\mathbf{G}_{qw}\|_2^2$ ($\mathbf{G}_{qw} = 0.0525$). (a) feedforward control. (b) feedback control.

The $\mathcal{H}_2$ system norm of the following two closed-loop transfer functions

$$\mathbf{T}_{qw} = \begin{bmatrix} \bar{C}_1 & 0 \end{bmatrix} (sI - \mathcal{A}_{cl})^{-1} \mathcal{B}_{cl}, \tag{29}$$

$$\mathbf{T}_{\phi w} = \begin{bmatrix} 0 & -\mathbf{F} \end{bmatrix} (sI - \mathcal{A}_{cl})^{-1} \mathcal{B}_{cl} \tag{30}$$

will be used as performance metric to design the controller. $\|\mathbf{T}_{qw}\|_2$ is the $\mathcal{H}_2$ closed-loop system norm from the external disturbances to the controlled output and is a measure for the control performance. $\|\mathbf{T}_{\phi w}\|_2$ is the closed-loop system norm from the external disturbances to the control input and is a measure for the control effort. These norms are related to the LQG cost function in Eq. (24) through

$$\mathcal{J}_{LQG} = \|\mathbf{T}_{zw}\|_2^2 = \|\mathbf{T}_{qw}\|_2^2 + l^2 \|\mathbf{T}_{\phi w}\|_2^2, \tag{31}$$

where $\mathbf{T}_{zw} = C_{cl} (sI - \mathcal{A}_{cl})^{-1} \mathcal{B}_{cl}$. Based on a convergence analysis for the closed-loop system norms [Eq. (29)-Eq. (30)], the order of the ROM and corresponding controller is chosen as $r = 30$. With this order the norms have converged to the norms of the closed-loop system with the full-order controller and there is no loss in performance due to the truncated dynamics. Figure 7 shows the contours of the $\mathcal{H}_2$ system norms and the relative energy norm with both feedforward control (a) and feedback control (b) as function of the design parameters (γ, l) for the order

$r = 30$ controller. Since no uncertainties are explicitly accounted for in the control design, the combined feedforward/feedback set-up results in the same contours as the feedforward controller, i.e. feedforward information alone is sufficiently to reach its design performance. Due to the separation principle of the control design, the state feedback and state estimator can be tuned independently through l and γ. A low value for the control penalty l gives an improved performance at the cost of a higher control effort (higher state feedback gain $\mathbf{F}$). A low value for γ reflects a low output uncertainty. This gives an improved estimator performance at the cost of a reduced robustness in case of unmodeled measurement inaccuracies. Note that γ models a relative magnitude of the sensor noise, a convenient means to account for inaccuracies in the control design. The true magnitude of the noise will be substantially different for pressure sensors, which typically measure in Volts. Any sensor calibration, e.g. Volts to Pascal, will also change the magnitude of the noise. Therefore no conclusions can be drawn regarding robustness to sensor inaccuracies based on the magnitudes of γ in Fig. 7.

It can be observed that both feedback and feedforward control are able to achieve an energy reduction of two orders of magnitude from a design perspective. However, feedback control has a reduced nominal performance for a given l and γ and requires a higher control effort as compared to feedforward control. This can be attributed to the fact that feedforward control is able to act earlier on the incoming perturbations. The benefit of feedback control is that the controller senses the effectiveness of the control, possibly resulting in an improved performance in off-design conditions. On the other hand, closed-loop instabilities may be an issue [24] and $\mathcal{H}_2/LQG$ optimal controllers have no guaranteed stability margins [54]. To investigate the effect of the controller tuning on both the closed-loop performance and the closed-stability, two control design points are evaluated: an aggressive controller characterized by (I) $l = 0.025, \gamma = 0.04$ and a more conservative controller characterized by (II) $l = 0.05, \gamma = 0.2$. In selecting the more conservative controller, robustness to output uncertainties is given priority.

VII. Results

The selected controllers are evaluated using linear simulations of the closed-loop system. The model defining a plate with a total length of $L_{sim} = 400$ as discussed in Sec. B is used for simulating the response of the closed-loop system. All simulations are performed with a sampling time of $\Delta t = \Delta t^* \delta_0^* / U_0^* = 0.2$. The performance is studied for exponentially growing perturbations introduced using optimal initial conditions. The initial condition is optimized to provide the maximum energy growth

$$G(t) = \frac{E(t)}{E(0)} = \max_{\boldsymbol{u}_0} \frac{\|\boldsymbol{u}\|_{L^2}^2}{\|\boldsymbol{u}_0\|_{L^2}^2} = \max_{\|\boldsymbol{u}_0\|_{L^2}^2 = 1} \|\boldsymbol{u}\|_{L^2}^2 \tag{32}$$

at the given final time $t_{max} = 700$. At this final time the initial condition is spatially localized upstream of the control region. The initiation of the perturbations is independent of the disturbance model used to design the controller. It

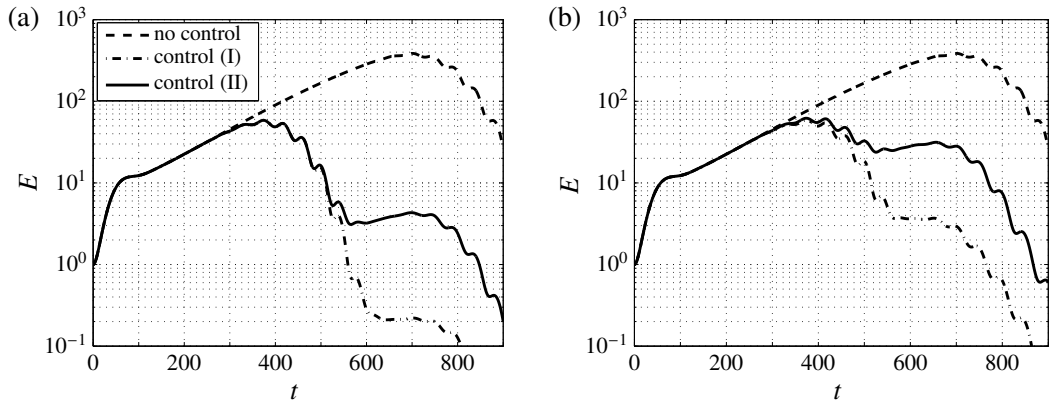

Fig. 8 Uncontrolled and controlled energy for the optimal perturbation at $Re = 500$, $m = -0.02$. (a) feedforward control . (b) feedback control.

provides a good benchmark to evaluate the effectiveness of the proposed control design [18], because the controller is not designed specifically for this perturbation scenario and it only has a limited window in time to counteract the perturbations that are propagating through the control domain in the form of a localized wavepacket. In addition this perturbation case allows the proper evaluation of the state estimator performance as the perturbations convect through the localized control domain. For the design of the estimator the problem is scaled in terms of γ. The role of γ is to account for uncertainties in the control design. First the nominal performance without uncertainties is evaluated in Sec. A. The effect of uncertainties in the Reynolds number and the pressure gradient is discussed in Sec. B.

A. Nominal performance

First the nominal performance ($Re_0 = 500$, $m = -0.02$) of the feedforward and feedback controllers is evaluated. The two control design points characterized by (I) $l = 0.025$, $\gamma = 0.04$ and (II) $l = 0.05$, $\gamma = 0.2$ are considered, see also Fig. 7. Since no dynamic uncertainties are present, the combined feedforward/feedback controller gives the same performance as compared to the feedforward controller; feedforward control alone is sufficient to achieve its design performance. The combined feedforward/feedback case is therefore only considered in the next section. Fig. 8 shows the perturbation energy growth as function of time with both feedforward control (a) and feedback control (b). The input-output signals, which are the feedforward pressure measurement $p_{ff}(t)$, the feedback pressure measurement $p_{fb}(t)$, the amplitude of the blowing and suction $\phi(t)$ and the controlled output $q(t)$, for the conservative controller (II) are shown in Fig. 9. The controlled output $q(t)$ reflects the controller performance as it is used within the control objective that is minimized by the controller. The spatio-temporal evolution of the perturbation and the performance of the state-estimator for controller (II) is visualized in Fig. 10. It shows a contour plot of the uncontrolled, controlled and estimated pressure at the wall $p_{wall}(x)$ for both the feedforward (a) and the feedback (b) control cases. The wall pressure is computed from the perturbation velocity through the linearized pressure Poisson equation, see Sec. V.

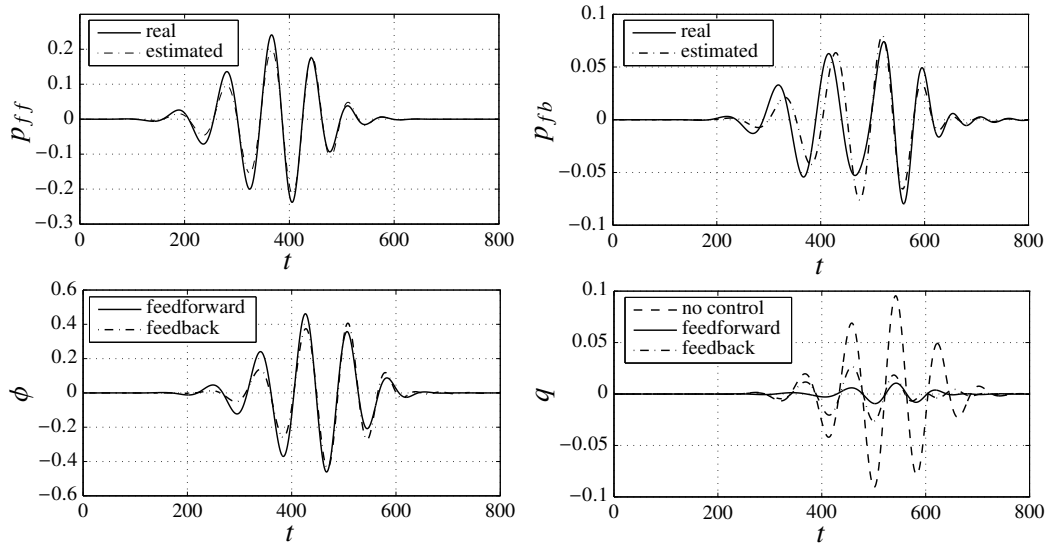

Fig. 9 Input-output signals for control of the optimal perturbation at $Re = 500$, $m = -0.02$. Conservative controller (II) is considered.

The initial perturbation for the uncontrolled case leads to an energy amplification of $G(t_{max}) \approx 3 \times 10^2$. After an initial transient growth the perturbation quickly develops into an exponentially growing wavepacket that propagates downstream. The energy of the uncontrolled wavepacket reaches a maximum at $t = 700$ after which it decays again as the wavepacket leaves the computational domain $x_{sim} \in [0, 400]$. The performance of the feedforward and feedback controllers is according to their design: The feedforward controllers achieve an energy reduction of two orders (control (I)) and three orders (control (II)) of magnitude. Controller (II) is more conservative as it takes higher output uncertainties into account. The feedback controller has a reduced nominal performance as it measures the incoming perturbations after it has convected passed the actuator. The unsteady actuator effect is clearly visible. The actuator effect is spatially localized and the controller only has a limited window in time ($200 < t < 600$) to cancel the incoming perturbations. After this control window the remaining perturbation has the opportunity to develop and to amplify again, see also Fig. 10. The control input confirms the filtering and feedback of the measurement to minimize the wall shear stress fluctuations defined by q. By minimizing q the amplitude of the perturbations is reduced in the entire region downstream of the control domain.

Fig. 10 also visualizes the performance of the localized state-estimator. The location of the sensor (feedback or feedforward) affects the observable region in which the perturbations is estimated. Note that the Kalman filter also estimates upstream perturbations as these contribute to the input-output behavior. It estimates both the effect of the control and the effect of upstream disturbances which are accounted for in the modeling and control design. The feedback controller is able to estimate the perturbations in the actuator domain since the feedback sensor is placed closely behind the actuator. The outflow boundary condition [Eq. (5f)] has an artificial effect on the state estimates

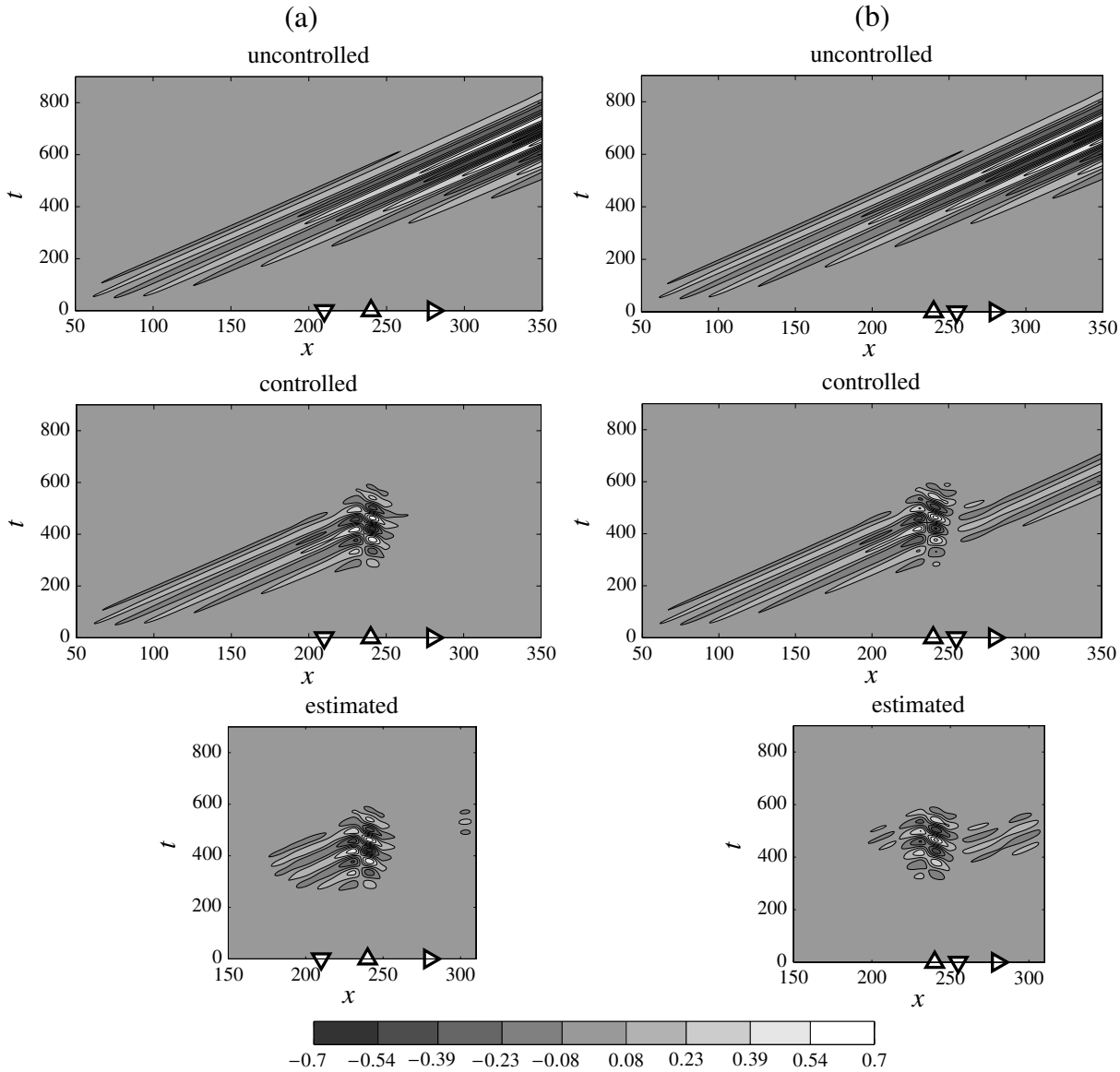

Fig. 10 Uncontrolled, controlled and estimated wall pressure $p_{wall}(x)$ of conservative controller (II). (a) Feed-forward control. (b) feedback control. Measurement sensor (▽), actuator (△) and controlled output (▷).

near the outflow of the control domain $x = 310$. However, this does not affect the estimates in the actuator/sensor region in which the perturbations are very well reconstructed. As a result the control is able to effectively dampen the incoming perturbations.

B. Robustness

When applying the controller in a real application, modeling uncertainties are unavoidable and potentially deteriorate the nominal performance. Robustness is the ability of the controller to overcome differences/uncertainties between the actual system and the model used for controller synthesis. The controller is designed in an optimal control frame-

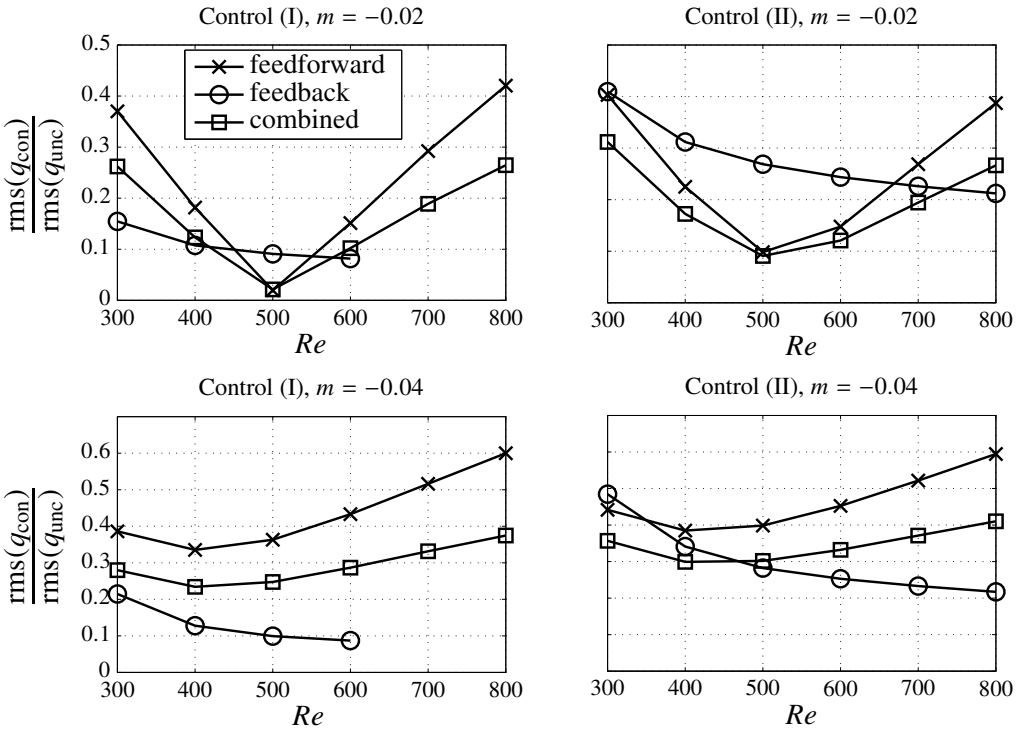

Fig. 11 Robustness analysis: effect of Reynolds number and pressure gradient on the control performance. Feedback control (I) is unstable for $Re = 700, 800$.

work and uncertainties are not directly taken into account in the control design as would be the case for a robust controller. However, the behavior of the controller can nonetheless be robust to deviations of the flow parameters, which is investigated in this section. In Belson et al. [24] the robustness of feedforward control and feedback control was evaluated in the presence of unmodeled disturbances. In this section also a combined feedforward/feedback configuration is considered and the robustness is evaluated in the presence of parametric uncertainties in the Reynolds number and the pressure gradient characterized by the parameter m. To also investigate the controller tuning on the robustness, the design points (I) and (II) are considered for all three configurations. The performance of the (in total six) controllers is evaluated by comparing the ratio between the rms of the controlled and uncontrolled performance signal $\mathrm{rms}(q_{\mathrm{con}})/\mathrm{rms}(q_{\mathrm{unc}})$. The results are summarized in Fig. 11. In addition to support the interpretation of the results, the response of the perturbation energy for the off-design case $Re = 800$, $m = -0.02$ is shown in Fig. 12. The following observations can be made.

Feedforward control gives the best nominal performance. However, it is also the most sensitive to uncertainties and a progressive loss of performance is observed for deviations from the nominal designed conditions $Re = 500$, $m = -0.02$. This can be attributed to the different speed, spatial wavelength and growth of the wavepacket. This makes the control out of phase with the perturbations. Nevertheless, the controller provides an amplitude reduction and does not destabilize the flow in case of large uncertainties (robust stability is guaranteed). For example, for the case

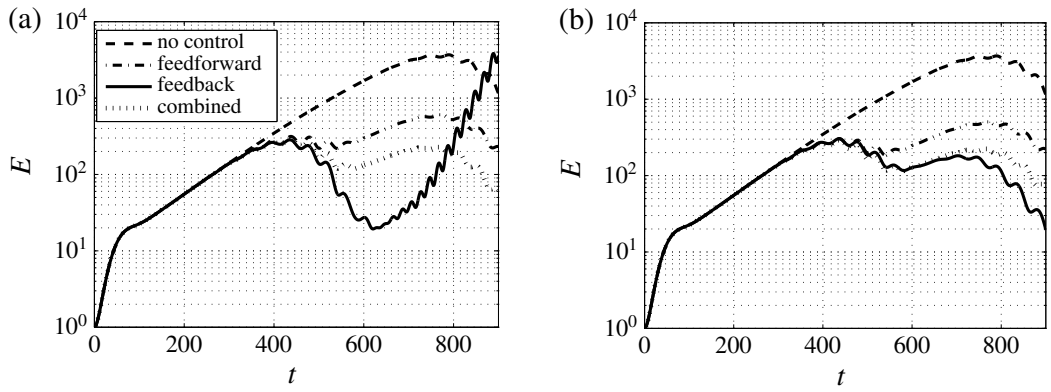

Fig. 12 Uncontrolled and controlled energy for the optimal perturbation at $Re = 800$, $m = -0.02$. (a) Control (I). (b) Control (II)

$Re = 800$, $m = -0.04$ the controller reduces the rms of q with 40%.

Feedback control has a reduced nominal performance, but it is better able to preserve this nominal performance in off-design conditions. However, closed-loop instability is of concern. In case of small parameter variations the aggressive feedback controller (I) gives the best performance, but it becomes unstable for $Re = 700$ and higher, see also Fig. 12. Feedback controller (II) takes higher output uncertainties into account and results in stable closed-loop control and a better performance at larger parameter uncertainties. In short, feedback control results in a better performance in off-design conditions but requires a more careful tuning of the controller to maintain stability of the closed-loop.

Combined feedforward/feedback gives the same nominal performance as feedforward control, but a better robust performance in off-design conditions. Still a progressive loss is observed for deviations from the designed conditions. This can be attributed to the fact that it initially acts on feedforward information. However, the loss in performance is significantly less as compared to feedforward control only due to the action of the additional feedback. In addition the stability is enhanced as compared to feedback control only. Also the aggressive controller (I) results in stable closed-loop control in the presence of large parameter uncertainties. Overall it is found that feedforward/feedback control gives the best trade-off between nominal performance, robust performance and robust stability.

VIII. Conclusion

In practical flow control applications, real-time measurements can only be obtained via sensors at discrete locations at the wall. Especially pressure-based sensors are technically attractive by ensuring that the associated costs of active flow control are positively balanced by net power savings. However, in past studies, implementation of pressure sensing in control design has not been treated in a systematic way as part of the control design methodology. In this paper the problem of point pressure output feedback control of 2-D boundary layer instabilities is addressed. A

new approach is presented to design and synthesize reduced-order compensators for estimation and control directly from the governing equations. The use of pressure measurements for dynamic flow estimation gives rise to additional modeling difficulties and output uncertainties as the pressure at a single point is related to the global flow field. The input-output behavior, which forms the basis for the estimation strategy, between the external flow perturbations and the pressure at wall is obtained using a novel method based on the inversion of the linearized pressure Poisson equation. This allows to relate the measured pressure at the wall with the global perturbation field. The results show that the dynamic estimation strategy (Kalman filter) is capable of obtaining accurate time-resolved estimates of the convective perturbation field in the localized control domain from pressure measurements at a single location at the wall.

The optimal LQG controller is designed in both a feedforward, a feedback and a combined feedforward/feedback actuator/sensor configuration. A comparison study is performed for the three configurations on aspects of nominal performance, robust performance and robust stability in the presence of parametric model uncertainties in the Reynolds number and pressure gradient. This is the first time that the robustness of a combined feedforward/feedback configuration is evaluated and it is shown that this configuration achieves the best trade-off between robust stability and robust performance. While feedback control outperforms feedforward control in the presence of uncertainties, it requires careful tuning of the controller to maintain stability of the closed-loop. Combined feedforward/feedback control enhances stability of the closed-loop compared to feedback control and it gives a better robust performance compared to feedforward control in off-design conditions. It should be noted that uncertainties are not directly accounted for in the control design and LQG control provides no guarantees on the stability of the closed-loop in the presence of uncertainties. In this study the effect of uncertainties on the stability and performance is assessed from case to case. However, the framework in this paper can also be used to synthesize robust controllers with a priory stability guarantees in off-design conditions, e.g. using $\mathcal{H}_\infty$ and μ-synthesis techniques.

The next step is aimed at applying the controller in experiments. This work has addressed important issues related to this next step, including modeling of the input-output dynamics and obtaining experimentally feasible low-order controllers with sufficient robustness, and thus provides an important step forwards for transition delay in boundary layer flows.

References

[1] Kim, J., and Bewley, T. R., "A linear systems approach to flow control," *Annual Review Fluid Mechanics*, Vol. 39, 2007, pp. 383–417. doi:10.1146/annurev.fluid.39.050905.110153.

[2] Bagheri, S., and Henningson, D. S., "Transition delay using control theory," *Philosophical Transactions of the Royal Society of London A: Mathematical, Physical and Engineering Sciences*, Vol. 369, No. 1940, 2011, pp. 1365–1381. doi:10.1098/rsta.2010.0358.

[3] Sipp, D., and Schmid, P. J., "Linear closed-loop control of fluid instabilities and noise-induced perturbations: A review of approaches and tools," *Applied Mechanics Reviews*, Vol. 68, No. 2, 2016, p. 020801. doi:10.1115/1.4033345.

[4] Högberg, M., Bewley, T. R., and Henningson, D. S., "Linear feedback control and estimation of transition in plane channel flow," *Journal of Fluid Mechanics*, Vol. 481, 2003, pp. 149–175. doi:10.1017/S0022112003003823.

[5] Högberg, M., Chevalier, M., and Henningson, D. S., "Linear compensator control of a pointsource induced perturbation in a Falkner-Skan-Cooke boundary layer," *Physics of Fluids*, Vol. 15, No. 8, 2003, pp. 2449–2452. doi:10.1063/1.1584434.

[6] Chevalier, M., Hœpffner, J., Åkervik, E., and Henningson, D. S., "Linear feedback control and estimation applied to instabilities in spatially developing boundary layers," *Journal of Fluid Mechanics*, Vol. 588, 2007, p. 163. doi:10.1017/S0022112007007392.

[7] Bagheri, S., Brandt, L., and Henningson, D. S., "Input–output analysis, model reduction and control of the flat-plate boundary layer," *Journal of Fluid Mechanics*, Vol. 620, 2009, pp. 263–298. doi:10.1017/S0022112008004394.

[8] Dadfar, R., Semeraro, O., Hanifi, A., and Henningson, D. S., "Output feedback control of blasius flow with leading edge using plasma actuator," *AIAA journal*, Vol. 51, No. 9, 2013, pp. 2192–2207. doi:10.2514/1.J052141.

[9] Brunton, S. L., and Noack, B. R., "Closed-loop turbulence control: progress and challenges," *Applied Mechanics Reviews*, Vol. 67, No. 5, 2015, p. 050801. doi:10.1115/1.4031175.

[10] Rowley, C. W., and Dawson, S. T. M., "Model reduction for flow analysis and control," *Annual Review of Fluid Mechanics*, Vol. 49, 2017, pp. 387–417. doi:10.1146/annurev-fluid-010816-060042.

[11] Barbagallo, A., Sipp, D., and Schmid, P. J., "Closed-loop control of an open cavity flow using reduced-order models," *Journal of Fluid Mechanics*, Vol. 641, 2009, pp. 1–50. doi:10.1017/S0022112009991418.

[12] Bagheri, S., Henningson, D. S., Hoepffner, J., and Schmid, P. J., "Input-output analysis and control design applied to a linear model of spatially developing flows," *Applied Mechanics Reviews*, Vol. 62, No. 2, 2009, p. 020803. doi:10.1115/1.3077635.

[13] Ilak, M., and Rowley, C. W., "Modeling of transitional channel flow using balanced proper orthogonal decomposition," *Physics of Fluids (1994-present)*, Vol. 20, No. 3, 2008, p. 034103. doi:10.1063/1.2840197.

[14] Moore, B. C., "Principal component analysis in linear systems: Controllability, observability, and model reduction," *IEEE Transactions on Automatic Control*, Vol. 26, No. 1, 1981, pp. 17–32. doi:10.1109/TAC.1981.1102568.

[15] Rowley, C. W., "Model reduction for fluids, using balanced proper orthogonal decomposition," *International Journal of Bifurcation and Chaos*, Vol. 15, No. 03, 2005, pp. 997–1013. doi:10.1142/S0218127405012429.

[16] Juang, J. N., and Pappa, R. S., "An eigensystem realization algorithm for modal parameter identification and model reduction," *Journal of guidance, control, and dynamics*, Vol. 8, No. 5, 1985, pp. 620–627. doi:10.2514/3.20031.

[17] Ma, Z., Ahuja, S., and Rowley, C. W., "Reduced-order models for control of fluids using the eigensystem realization algorithm," *Theoretical and Computational Fluid Dynamics*, Vol. 25, No. 1-4, 2011, pp. 233–247. doi:10.1007/s00162-010-0184-8.

[18] Bagheri, S., Åkervik, E., Brandt, L., and Henningson, D. S., "Matrix-free methods for the stability and control of boundary layers," *AIAA journal*, Vol. 47, No. 5, 2009, pp. 1057–1068. doi:10.2514/1.41365.

[19] Semeraro, O., Bagheri, S., Brandt, L., and Henningson, D. S., "Feedback control of three-dimensional optimal disturbances using reduced-order models," *Journal of Fluid Mechanics*, Vol. 677, 2011, pp. 63–102. doi:10.1017/S0022112011000620.

[20] Semeraro, O., Bagheri, S., Brandt, L., and Henningson, D. S., "Transition delay in a boundary layer flow using active control," *Journal of Fluid Mechanics*, Vol. 731, 2013, pp. 288–311. doi:10.1017/jfm.2013.299.

[21] Dadfar, R., Hanifi, A., and Henningson, D. S., "Feedback Control for Laminarization of flow over Wings," *Flow, Turbulence and Combustion*, Vol. 94, No. 1, 2015, pp. 43–62. doi:10.1007/s10494-014-9578-9.

[22] Fabbiane, N., Simon, B., Fischer, F., Grundmann, S., Bagheri, S., and Henningson, D. S., "On the role of adaptivity for robust laminar flow control," *Journal of Fluid Mechanics*, Vol. 767, 2015, p. R1. doi:10.1017/jfm.2015.45.

[23] Schmid, P. J., and Sipp, D., "Linear control of oscillator and amplifier flows," *Phys. Rev. Fluids*, Vol. 1, 2016, p. 040501. doi:10.1103/PhysRevFluids.1.040501.

[24] Belson, B. A., Semeraro, O., Rowley, C. W., and Henningson, D. S., "Feedback control of instabilities in the two-dimensional Blasius boundary layer: The role of sensors and actuators," *Physics of Fluids (1994-present)*, Vol. 25, No. 5, 2013, p. 054106. doi:10.1063/1.4804390.

[25] Juillet, F., McKeon, B. J., and Schmid, P. J., "Experimental control of natural perturbations in channel flow," *Journal of Fluid Mechanics*, Vol. 752, 2014, pp. 296–309. doi:10.1017/jfm.2014.317.

[26] Sheplak, M., Cattafesta, L., Nishida, T., and McGinley, C., "MEMS shear stress sensors: promise and progress," *24th AIAA Aerodynamic Measurement Technology and Ground Testing Conference*, 2004, p. 2606. doi:10.2514/6.2004-2606.

[27] Cattafesta, L. N., Song, Q., Williams, D. R., Rowley, C. W., and Alvi, F. S., "Active control of flow-induced cavity oscillations," *Progress in Aerospace Sciences*, Vol. 44, No. 7, 2008, pp. 479–502. doi:10.1016/j.paerosci.2008.07.002.

[28] Adrian, R. J., "On the role of conditional averages in turbulence theory," *Turbulence in Liquids*, Vol. 1, 1977, pp. 323–332.

[29] Murray, N. E., and Ukeiley, L. S., "Estimation of the flowfield from surface pressure measurements in an open cavity," *AIAA journal*, Vol. 41, No. 5, 2003, pp. 969–972. doi:10.2514/2.2035.

[30] Samimy, M., Debiasi, M., Caraballo, E., Serrani, A., Yuan, X., Little, J., and Myatt, J. H., "Feedback control of subsonic cavity flows using reduced-order models," *Journal of Fluid Mechanics*, Vol. 579, 2007, pp. 315–346. doi:10.1017/S0022112007005204.

[31] Sinha, A., Serrani, A., and Samimy, M., "Development of empirical estimators for feedback control of high-speed axisymmetric jets," *AIAA journal*, Vol. 49, No. 9, 2011, pp. 1971–1987. doi:10.2514/1.J050966.

[32] Lasagna, D., Orazi, M., and Iuso, G., "Multi-time delay, multi-point linear stochastic estimation of a cavity shear layer velocity from wall-pressure measurements," *Physics of Fluids*, Vol. 25, No. 1, 2013, p. 017101. doi:10.1063/1.4774337.

[33] Ukeiley, L., Murray, N., Song, Q., and Cattafesta, L., "Dynamic surface pressure based estimation for flow control," *IUTAM Symposium on Flow Control and MEMS*, Springer, 2008, pp. 183–189. doi:10.1007/978-1-4020-6858-4.

[34] Rowley, C. W., and Juttijudata, V., "Model-based control and estimation of cavity flow oscillations," *Decision and Control, 2005 and 2005 European Control Conference. CDC-ECC'05. 44th IEEE Conference on*, IEEE, 2005, pp. 512–517. doi:10.1109/CDC.2005.1582207.

[35] Illingworth, S. J., Morgans, A. S., and Rowley, C. W., "Feedback control of flow resonances using balanced reduced-order models," *Journal of Sound and Vibration*, Vol. 330, No. 8, 2011, pp. 1567–1581. doi:10.1016/j.jsv.2010.10.030.

[36] Illingworth, S. J., Morgans, A. S., and Rowley, C. W., "Feedback control of cavity flow oscillations using simple linear models," *Journal of Fluid Mechanics*, Vol. 709, 2012, pp. 223–248. doi:10.1017/jfm.2012.330.

[37] Jones, B. L., Heins, P. H., Kerrigan, E. C., Morrison, J. F., and Sharma, A. S., "Modelling for robust feedback control of fluid flows," *Journal of Fluid Mechanics*, Vol. 769, 2015, pp. 687–722. doi:10.1017/jfm.2015.84.

[38] Bewley, T. R., Temam, R., and Ziane, M., "A general framework for robust control in fluid mechanics," *Physica D: Nonlinear Phenomena*, Vol. 138, No. 3-4, 2000, pp. 260–392. doi:10.1016/S0167-2789(99)00206-7.

[39] Tol, H. J., Kotsonis, M., de Visser, C. C., and Bamieh, B., "Localised estimation and control of linear instabilities in two-dimensional wall-bounded shear flows," *Journal of Fluid Mechanics*, Vol. 824, 2017, pp. 818–865. doi:10.1017/jfm.2017.355.

[40] Tol, H. J., de Visser, C. C., and Kotsonis, M., "Model reduction of parabolic PDEs using multivariate splines," *International Journal of Control*, 2016. doi:10.1080/00207179.2016.1222554.

[41] Doyle, J. C., Glover, K., Khargonekar, P. P., and Francis, B., "State-space solutions to standard H_2 and H_∞ control problems," *Automatic Control, IEEE Transactions on*, Vol. 34, No. 8, 1989, pp. 831–847.

[42] Heywood, J. G., Rannacher, R., and Turek, S., "Artificial boundaries and flux and pressure conditions for the incompressible Navier–Stokes equations," *International Journal for numerical methods in fluids*, Vol. 22, No. 5, 1996, pp. 325–352. doi:10.1002/(SICI)1097-0363(19960315)22:5<325::AID-FLD307>3.0.CO;2-Y.

[43] Curtain, R. F., and Zwart, H. J., *An introduction to infinite-dimensional linear systems theory*, Springer-Verlag, New York, 1995. doi:10.1007/978-1-4612-4224-6.

[44] Högberg, M., and Henningson, D. S., "Linear optimal control applied to instabilities in spatially developing boundary layers," *Journal of Fluid Mechanics*, Vol. 470, 2002, pp. 151–179. doi:10.1017/S0022112002001702.

[45] Joshi, S. S., Speyer, J. L., and Kim, J., "A systems theory approach to the feedback stabilization of infinitesimal and finite-amplitude disturbances in plane Poiseuille flow," *Journal of Fluid Mechanics*, Vol. 332, 1997, pp. 157–184. doi:10.1017/S0022112096003746.

[46] Farin, G., "Triangular Bernstein-Bézier patches," *Computer Aided Geometric Design*, Vol. 3, No. 2, 1986, pp. 83–127. doi:10.1016/0167-8396(86)90016-6.

[47] de Boor, C., "B-form Basics," *Geometric Modeling: Algorithms and New Trends*, edited by G. Farin, SIAM, Philadelphia, 1987, pp. 131–148.

[48] Lai, M. J., and Schumaker, L. L., *Spline functions on triangulations*, 110, Cambridge University Press, 2007. doi:10.1017/CBO9780511721588.

[49] Awanou, G., and Lai, M. J., "Trivariate spline approximations of 3D Navier-Stokes equations," *Mathematics of computation*, Vol. 74, No. 250, 2004, pp. 585–601. doi:10.1090/S0025-5718-04-01715-6.

[50] Schmid, P. J., and Henningson, D. S., *Stability and Transition in Shear Flows*, Springer, 2001. doi:10.1007/978-1-4613-0185-1.

[51] Chevalier, M., Lundbladh, A., and Henningson, D. S., "SIMSON–A pseudo-spectral solver for incompressible boundary layer flow," Tech. rep., KTH Royal Institute of Technology in Stockholm, 2007.

[52] Zhou, K., Doyle, J. C., and Glover, K., *Robust and optimal control*, Prentice hall New Jersey, 1996.

[53] Bewley, T. R., and Liu, S., "Optimal and robust control and estimation of linear paths to transition," *Journal of Fluid Mechanics*, Vol. 365, 1998, pp. 305–349. doi:10.1017/S0022112098001281.

[54] Doyle, J., "Guaranteed margins for LQG regulators," *IEEE Transactions on Automatic Control*, Vol. 23, No. 4, 1978, pp. 756–757. doi:10.1109/TAC.1978.1101812.